

## Concurrent triple-scale simulation of molecular liquids

Rafael Delgado-Buscalioni,<sup>1,a)</sup> Kurt Kremer,<sup>2,b)</sup> and Matej Praprotnik<sup>2,c)</sup>

<sup>1</sup>*Departamento Física Teórica de la Materia Condensada, Universidad Autónoma de Madrid, Campus de Cantoblanco, Madrid, E-28049, Spain*

<sup>2</sup>*Max-Planck-Institut für Polymerforschung, Ackermannweg 10, D-55128 Mainz, Germany*

(Received 17 January 2008; accepted 12 February 2008; published online 20 March 2008)

We present a triple-scale simulation of a molecular liquid, in which the atomistic, coarse-grained, and continuum descriptions of the liquid are concurrently coupled. The presented multiscale approach, which covers the length scales ranging from the micro- to macroscale, is a combination of two dual-scale models: a particle-based adaptive resolution scheme (AdResS), which couples the atomic and mesoscopic scales, and a hybrid continuum-molecular dynamics scheme (HybridMD). The combined AdResS-HybridMD scheme successfully sorts out the problem of large molecule insertion in the hybrid particle-continuum simulations of molecular liquids. The combined model is shown to correctly describe the hydrodynamics within a hybrid particle-continuum framework. The presented approach opens up the possibility to perform efficient grand-canonical molecular dynamics simulations of truly open molecular liquid systems. © 2008 American Institute of Physics. [DOI: 10.1063/1.2890729]

### I. INTRODUCTION

Many processes in molecular liquids and soft matter are inherently multiscale, i.e., they involve a range of different time and length scales that are intrinsically interconnected. The relevant properties of the system are thus typically determined by the interplay of the various temporal and spatial scales involved. All-atom simulations that capture phenomena on the atomic scale are often not computationally feasible or even not desirable due to a large number of the degrees of freedom (DOFs) in these systems. The more coarse-grained models or continuum simulations, on the other hand, can cover much larger time and length scales but are unable to provide the information on the atomic level of detail. Multiscale modeling techniques that concurrently couple different length scales, where each separate scale is described by the appropriate model for that particular scale, hence, providing a very efficient way to treat such systems by a computer simulation.<sup>1</sup> Using a multiscale approach one simplifies the model of the physical system to the largest extent possible while keeping all the necessary details of the system where this is required.

Such hybrid multiscale methods have been developed and successfully applied to study solid state systems, where the atomistic simulation was either combined with the finite elements method<sup>2–6</sup> or it was linked to a quantum mechanical model.<sup>7,8</sup> In recent years there have been a few schemes also derived for hybrid atomistic-continuum simulations of molecular fluids where an atomistic domain has been embedded into the continuum hydrodynamics domain described either by the deterministic<sup>9–18</sup> or the fluctuating Navier–Stokes equations.<sup>19,20</sup> However, one problem of this class of hybrid

methods, when applied to molecular fluids, is the insertion of complex molecules into a dense liquid at the molecular (atomistic)/continuum boundary. Because of that the applications have been limited so far to “simple” liquids such as the Lennard-Jones fluid<sup>21</sup> or water.<sup>22</sup>

In parallel, there have been recent efforts made to concurrently couple atomic and coarse-grained scales within the class of the particle-based methods, see for example Refs. 23–27. There the molecules adaptively on-the-fly change their level of resolution from the atomic to coarse-grained one and vice versa on demand during the course of a single molecular dynamics (MD) or Monte Carlo simulation. Thus far, these simulations could only be performed in the canonical statistical ensemble with a constant number of molecules in the system. Moreover, previous work on this particle-based method did not explicitly include hydrodynamic transport of mass and momentum. An extension allowing simulation of open systems in the grand-canonical ensemble and including hydrodynamic transfer across the atomic and different coarse-grained scales involved, would thus very much enlarge the scope and applicability of this kind of multiscale simulations.

In this work, we combine the two dual-scale approaches, i.e., the particle-based adaptive resolution scheme<sup>23–25</sup> (AdResS) and hybrid continuum-molecular dynamics (HybridMD).<sup>19,20</sup> The combined approach solves the problem of large molecule insertion in the hybrid particle-continuum simulations of molecular liquids and at the same time extends the applicability of the particle-based adaptive resolution schemes to simulate open systems in the grand-canonical ensemble including hydrodynamic coupling with the outer flow.

### II. LIQUID MODEL

The modeled system is an open particle system of tetrahedral molecules<sup>23–25</sup> in a liquid state schematically pre-

<sup>a)</sup>Electronic mail: rafael.delgado@uam.es.

<sup>b)</sup>Electronic mail: kremer@mpip-mainz.mpg.de.

<sup>c)</sup>Electronic mail: praprot@mpip-mainz.mpg.de. On leave from the National Institute of Chemistry, Hajdrihova 19, SI-1001 Ljubljana, Slovenia.

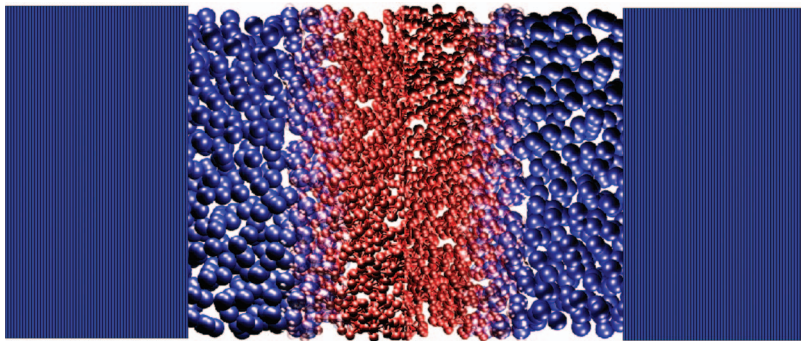


FIG. 1. (Color) The triple-scale model of the tetrahedral molecules' liquid. The molecular particle-based region is embedded in the hydrodynamics continuum. The molecular region is divided into the central explicit atomistic (ex) region with molecules represented using the atomic resolution (red tetrahedral molecules) sandwiched in between two coarse-grained (cg) domains with the molecules represented on a more coarse-grained level of detail (one particle blue molecules). The molecules freely move between the three levels of resolution and change their resolution accordingly.

sented in Fig. 1. The triple-scale system is divided into a molecular particle-based micro-mesoscopic region, which is surrounded by a liquid described on the macroscopic continuum level. The molecular region is further split into the central explicit atomistic (ex) region, where the molecules are modeled using atomic resolution, and the surrounding (cg) part modeled on a more coarse-grained level of detail. The ex region, which is our “region of interest” with the highest resolution, is thus occupied by atomistic tetrahedral molecules, while the cg region is filled up with the corresponding one particle coarse-grained molecules.

The liquid molecules in the ex regime are composed of four equal atoms with mass  $m_0$ . The atom diameter  $\sigma$  is fixed via the repulsive Weeks–Chandler–Andersen potential

$$U_{\text{rep}}^{\text{atom}}(r_{i\alpha j\beta}) = \begin{cases} 4\epsilon \left[ \left( \frac{\sigma}{r_{i\alpha j\beta}} \right)^{12} - \left( \frac{\sigma}{r_{i\alpha j\beta}} \right)^6 + \frac{1}{4} \right]; & r_{i\alpha j\beta} \leq 2^{1/6}\sigma \\ 0; & r_{i\alpha j\beta} > 2^{1/6}\sigma \end{cases}, \quad (1)$$

with the cutoff at  $2^{1/6}\sigma$ .  $\sigma$  and  $\epsilon$  are the standard Lennard-Jones units for lengths and energy, respectively. In what follows, all quantities shall be expressed in the standard Lennard-Jones units associated to the atoms: length  $\sigma$ , mass  $m_0$ , energy  $\epsilon$ , and time  $\tau \equiv \sigma(m_0/\epsilon)^{1/2}$ . The distance between the atom  $i$  of the molecule  $\alpha$  and the atom  $j$  of the molecule  $\beta$  is  $r_{i\alpha j\beta}$ . The neighboring atoms in a given molecule  $\alpha$  are connected by finite extensible nonlinear elastic bonds

$$U_{\text{bond}}^{\text{atom}}(r_{i\alpha j\alpha}) = \begin{cases} -\frac{1}{2}kR_0^2 \ln \left[ 1 - \left( \frac{r_{i\alpha j\alpha}}{R_0} \right)^2 \right]; & r_{i\alpha j\alpha} \leq R_0 \\ \infty; & r_{i\alpha j\alpha} > R_0 \end{cases}, \quad (2)$$

with divergence length  $R_0 = 1.5\sigma$  and stiffness  $k = 30\epsilon/\sigma^2$ , so that the average bond length is approximately  $0.97\sigma$  for  $k_B T = \epsilon$ , where  $T$  is the temperature of the system and  $k_B$  is Boltzmann's constant. For the coarse-grained model in the cg regime we use one-site spherical molecules interacting via an effective pair potential,<sup>23,24</sup> which was derived such that the statistical properties, i.e., the center of mass radial distribution function and pressure, of the high resolution liquid at a given phase point are accurately reproduced.<sup>28</sup> In this way the atomistically resolved part of the liquid is maintained at thermodynamical equilibrium with a liquid in the coarse-grained regime.<sup>29</sup> In our numerical tests we treat a medium

density liquid with a molecular number density of  $\rho_m = 0.1/\sigma^3 \approx 0.58/\sigma_{\text{cg}}^3$  and pressure  $p = 0.4\epsilon/\sigma^3$ , and a high density liquid with  $\rho_m = 0.175/\sigma^3 \approx 1.0/\sigma_{\text{cg}}^3$  and pressure  $p = 2.0\epsilon/\sigma^3$  ( $\sigma_{\text{cg}} \approx 1.8\sigma$  is the excluded volume diameter of the coarse-grained molecule<sup>24</sup>).

The two molecular regions freely exchange molecules through a transition regime (hyb) containing hybrid molecules,<sup>30</sup> where the molecules with no extra equilibration adapt their resolution and change the number of DOFs accordingly.<sup>23</sup> Furthermore, the cg region also exchanges molecules (that are annihilated/created in accordance with the grand-canonical ensemble) with the continuum part of the system. Thus, in the triple-scale model described earlier the liquid is modeled at each domain of the system only with the level of detail, which is absolutely necessary for that particular area. This allows for the most efficient description of the liquid with the least number of DOFs used but at the same time retaining all the necessary details in the model.

### III. ADAPTIVE RESOLUTION SCHEME

The dynamics of molecules in the molecular particle-based region of the system is governed by the classical Newton's equations of motion, which are solved using the MD simulation technique. The atomic and mesoscopic scales in the molecular particle-based region are smoothly coupled using the AdResS.<sup>23</sup> The transition between the two resolutions, which needs to be smooth for MD simulations, is governed by a weighting function  $w(x) \in [0, 1]$  that interpolates the interaction forces between the two regimes and assigns the identity of the particle. In the present work we employ the weighting function of the following form (see Fig. 2):

$$w(x) = \begin{cases} 0; & -a/2 - d > x \geq -l/2 \\ \cos^2 \left[ \frac{\pi}{2d}(x + a/2) \right]; & -a/2 > x \geq -a/2 - d \\ 1; & a/2 > x \geq -a/2 \\ \cos^2 \left[ \frac{\pi}{2d}(x - a/2) \right]; & a/2 + d > x \geq a/2 \\ 0; & l/2 \geq x \geq a/2 + d \end{cases}, \quad (3)$$

where  $l$ ,  $a$ , and  $d$  are widths of the molecular, atomistic (ex), and transition (hyb) regimes of the system, respectively.

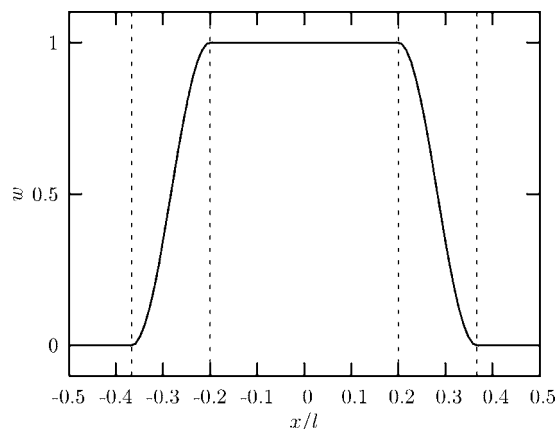


FIG. 2. The weighting function  $w(x) \in [0, 1]$  defined by Eq. (3). The values  $w=1$  and  $w=0$  correspond to the atomistic (ex) and coarse-grained (cg) regions, respectively, of the molecular region with the size  $l=15\sigma$ , whereas the values  $0 < w < 1$  correspond to the transition regime (hyb). Shown is the example where the widths of the hyb and ex regions are  $d=2.5\sigma$  and  $a=6\sigma$ , respectively. The vertical lines denote the boundaries of the hyb regime.

The weighting function given by Eq. (3) is defined in such a way that  $w=1$  corresponds to the atomistic (ex) region, and  $w=0$  to the coarse-grained (cg) region, whereas the values  $0 < w < 1$  correspond to the transition (hyb) regime. The atomic and mesoscopic length scales are coupled via the intermolecular force acting between centers of mass of molecule  $\alpha$  and  $\beta$  as

$$\mathbf{F}_{\alpha\beta} = w(X_\alpha)w(X_\beta)\mathbf{F}_{\alpha\beta}^{\text{atom}} + [1 - w(X_\alpha)w(X_\beta)]\mathbf{F}_{\alpha\beta}^{\text{cm}}, \quad (4)$$

where  $\mathbf{F}_{\alpha\beta}^{\text{atom}} = \sum_{i_\alpha j_\beta} \mathbf{F}_{i_\alpha j_\beta}^{\text{atom}} = -\sum_{i_\alpha j_\beta} \partial U^{\text{atom}} / \partial \mathbf{r}_{i_\alpha j_\beta}$  is the sum of all pair intermolecular atom interactions between explicit atoms of the molecules  $\alpha$  and  $\beta$  and  $\mathbf{F}_{\alpha\beta}^{\text{cm}} = -\partial U^{\text{cm}} / \partial \mathbf{R}_{\alpha\beta}$  is the corresponding effective intermolecular force between their centers of mass.  $\mathbf{r}_{i_\alpha j_\beta} = \mathbf{r}_{i_\alpha} - \mathbf{r}_{j_\beta}$  is the vector between atom  $i$  in molecule  $\alpha$  and atom  $j$  in molecule  $\beta$  and  $\mathbf{R}_{\alpha\beta} = \mathbf{R}_\alpha - \mathbf{R}_\beta$  is the vector between the centers of mass of molecules  $\alpha$  and  $\beta$ , with the corresponding  $X$  coordinates  $X_\alpha$  and  $X_\beta$ . To suppress the density fluctuations at the transition regime we employ the interface pressure correction.<sup>24</sup> Each time a molecule crosses a boundary between the different regimes it gains or loses (depending on whether it leaves or enters the coarse-grained region) its equilibrated rotational DOFs while retain-

ing its linear momentum. To supply or remove the latent heat caused by the switch of resolution and to synchronize the timescales of the all-atom and coarse-grained regimes in the molecular region while preserving the hydrodynamics this method is employed together with a combination of the standard and recently introduced Transverse dissipative particle dynamics (DPD) thermostats.<sup>31,32</sup> The application of the thermostats and proper derivation of the effective pair potential between coarse-grained molecules (yielding the same pressure in the ex and cg regions) provide the same chemical potential across the molecular region. This guarantees the free exchange of molecules between the ex and cg regions with a zero net flux.<sup>1,29</sup> As discussed in earlier publications, it is important to interpolate the forces and not the interaction potentials in order to satisfy Newton's Third Law.<sup>29,33,34</sup> This is crucial among others for the local linear momentum conservation.

A bottleneck for performing hybrid particle-continuum simulations of complex molecular liquids is the insertion of large molecules into a dense liquid<sup>21,22</sup> (see the next section). Exploiting the earlier described methodology one can solve this problem by gradually lowering the molecular resolution to the level at which the insertion of molecules is no longer problematic.

#### IV. HYBRID MOLECULAR-CONTINUUM HYDRODYNAMICS

The AdResS method presented in the previous section is a dual-scale approach based on domain decomposition whereby an atomistically described fluid domain (explicit model) is gradually converted into a coarse-grained molecular description as one moves outwards in space. As stated earlier, in this work we further expand this approach by connecting the coarse-grained domain with a continuum description of the external fluid flow.

The HybridMD is designed to connect the dynamics of a "molecular domain" with that obtained from a continuum description of the surrounding fluid flow. The method is based on flux exchange and it is explained in detail in Refs. 19 and 20. The idea is conceptually simple, as illustrated in Fig. 3. The system is divided in (at least) two domains, described via classical MD and continuum fluid dynamics (CFD). While at the particle domain each molecule's motion

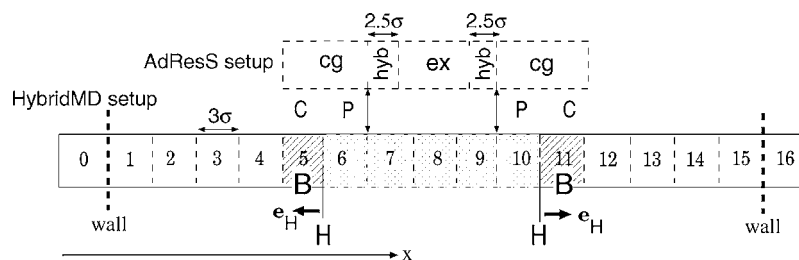


FIG. 3. Domain decomposition of the combined AdResS and HybridMD used in the present test cases. The top part of the figure shows the location of the fluid model layers (cg, hyb, and ex) within the HybridMD setup. The width of the hyb regime is  $2.5\sigma$ , which approximately corresponds to the range of the effective intermolecular interaction in the tetrahedral fluid (Refs. 23 and 24). The bottom part of the figure shows the set of control cells used in the HybridMD setup: the dotted region corresponds to the molecular domain, surrounded by a continuum description of the fluid flow (solved via the finite volume method). The shaded regions indicate the particle buffers  $B$ . The "P" and "C" cells adjacent to the hybrid interfaces  $H$  are also indicated. All the control cells are  $\Delta x=3\sigma$  wide in the (coupling)  $x$  direction, and  $15 \times 15\sigma^2$  in the orthogonal (periodic) directions. Cell number 0 and 16 are used to set the (no-slip, rigid wall) boundary conditions in the finite volume scheme.

is described via Newtonian dynamics ( $\mathbf{a}_i = \mathbf{f}_i/m_i$ ), at the CFD side we solve the Navier–Stokes equations. The MD and CFD components are coupled independent models, which exchange information after every fixed time interval  $\Delta t_c$ . We set  $\Delta t_c = n_{\text{CFD}} \Delta t = n_{\text{MD}} \delta t$ , where  $\Delta t$  and  $\delta t$  are the CFD and MD time steps and  $n_{\text{CFD}}$  and  $n_{\text{MD}}$  are integers which depend on the system being modeled.<sup>35</sup> The MD and CFD domains share one unique “hybrid interface,”  $H$ . Flux balance implies the conservation of mass and momentum across  $H$ : both domains should receive equal but opposite sign mass and momentum transfer across  $H$  over each  $\Delta t_c$ . In the HybridMD scheme the mass flux across the hybrid interface is not explicitly imposed, but naturally arises as a consequence of local pressure gradients, as occurs in hydrodynamics. Therefore, the central quantity, which drives mass and momentum exchange between the CFD and MD domains, is the momentum flux across  $H$ . This flux is equal to  $\mathbf{J}_H \cdot \mathbf{e}_H$ , where  $\mathbf{e}_H$  is the surface unit vector, normal to the  $H$  interface and  $\mathbf{J}_H$  is the local pressure tensor at  $\mathbf{r} = \mathbf{r}_H$  [i.e.,  $\mathbf{J}_H \equiv \mathbf{J}(\mathbf{r}_H, t)$ ]. The pressure tensor

$$\mathbf{J} = \rho \mathbf{v} \mathbf{v} + p \mathbf{I} + \mathbf{\Pi}, \quad (5)$$

includes a convective term (proportional to the dyadic product of the velocity  $\mathbf{v} \mathbf{v}$ ), the thermodynamic pressure  $p(\rho, T)$ , and the stress tensor  $\mathbf{\Pi} = -\eta [\nabla \mathbf{v}]^S - \xi \nabla \cdot \mathbf{v} \mathbf{I}$  (here  $\mathbf{I}$  is the identity matrix).<sup>36</sup> We consider a Newtonian fluid with dynamic viscosity  $\eta$  and bulk viscosity  $\xi$ .

In general, the HybridMD scheme allows to switch on hydrodynamic fluctuations at the CFD domain [in this case the pressure tensor in Eq. (5) includes an extra term arising from stress fluctuations<sup>19,20</sup>]. However, in this work hydrodynamic fluctuations are switched off at the CFD region in order to clearly assess the accuracy of the coupled AdResS-HybridMD scheme. In the Eulerian description of fluid dynamics the evolution of the local density of any conserved fluid variable, say  $\phi(\mathbf{r}, t)$ , is given by the conservation equation  $\partial \phi / \partial t = -\nabla \cdot \mathbf{J}^\phi$ , where  $\mathbf{J}^\phi(\mathbf{r}, t)$  is the associated local “flux.” We consider mass and momentum transfers so that the set of conserved densities is  $\phi = \{\rho, \rho \mathbf{v}\}$ . We solve this set of (Navier–Stokes) equations using the finite volume method. A detailed discussion of the CFD solver used in HybridMD was presented in Ref. 37 and here we briefly outline the method for the sake of completeness. The finite volume method is based on the spatial integration of the conservation equations within a discrete set  $k = \{1, \dots, N\}$  of nonoverlapping control cells of volume  $V_k$  which decompose the whole system (see Fig. 3). Integration within each volume gives

$$\frac{d\Phi_k}{dt} = - \sum_l \mathbf{J}_{kl}^\phi \cdot \mathbf{e}_{kl}, \quad (6)$$

where  $\mathbf{e}_{kl}$  is the surface vector of the  $kl$  interface (pointing toward the  $l$  cell) and  $\Phi_k = \int_{V_k} \phi(\mathbf{r}, t) d\mathbf{r}^3$  stands for the amount of  $\Phi$  at cell  $k$  at time  $t$ . In standard CFD, Eq. (6) is closed by the constitutive relations expressing the fluxes in terms of fluid variables and their gradients. In particular,  $\mathbf{J}^\rho = \rho \mathbf{v}$  is the mass flux, while the momentum flux is given by Eq. (5). The resulting discretized Navier–Stokes equations

are then integrated in time using a simple explicit Euler scheme.<sup>37</sup> As shown in Fig. 3, the interface  $H$  connects the “particle” cell  $P$  and the “continuum” cell  $C$ . The corresponding surface vector is thus  $\mathbf{e}_H \equiv \mathbf{e}_{PC} = -\mathbf{e}_{CP}$ , as indicated in Fig. 3.

As stated, one of the key issues in the hybrid scheme is to evaluate the momentum flux across the  $H$  interface,  $\mathbf{J}_H \cdot \mathbf{e}_H$ . This flux is used to update the flow variables at the CFD cells, according to Eq. (6). In turn, the same (but opposite sign) flux  $-\mathbf{J}_H \cdot \mathbf{e}_H$  needs to be imposed into the particle system across  $H$ . This point shall be explained later.

In the hybrid scheme one has a direct access to the microscopic dynamics so there are, in general, two ways to evaluate the momentum flux  $\mathbf{J}_H \cdot \mathbf{e}_H$ . One can use the microscopic expression (Irving–Kirkwood) for the pressure tensor (see Ref. 20). Alternatively, in this work we use a “mesoscopic approach,” which consists on using the local fluid variables at the MD cells<sup>38</sup> to evaluate momentum flux according to Eq. (5). Both (“micro” and “mesoscopic”) routes were shown to give similar results (in terms of mean and variance) in recent simulations coupling molecular dynamics and fluctuating hydrodynamics.<sup>20</sup> Note that the mesoscopic route avoids the cost of evaluating the microscopic stress and it also simplifies the structure of the coupling algorithm (one just needs to plug the local MD variables into the CFD equations). Finally, we note that the continuity of the velocity field at  $H$  is ensured by adding a relaxation term into the momentum equation of the CFD cells adjacent to  $H$  interface<sup>39</sup> (see Ref. 14 for details).

The way one imposes the momentum flux  $-\mathbf{J}_H \cdot \mathbf{e}_H$  into the particle system constitutes the core of the HybridMD algorithm. For that sake, hybrid schemes use a buffer domain  $B$ , which is shown in Fig. 3. It is important to note that the buffer  $B$  is not part of the system (which is just CFD+MD). In fact, the buffer acts as a mass and momentum reservoir for the particle region. It is also used to impose the external momentum into MD: molecules are free to enter or leave  $B$  across  $H$ , but once inside  $B$  each particle feels an external force  $\mathbf{f}_i^{\text{ext}}$  such that  $\mathbf{F}^{\text{ext}} = \sum_{i \in B} \mathbf{f}_i^{\text{ext}} = -A \mathbf{J}_H \cdot \mathbf{e}_H$  (here  $A$  is the area of the  $H$  interface). This external force includes pressure, shear, and inertial forces from outside and can be spatially distributed in different ways (for example, so as to achieve a flat density profile over the whole buffer<sup>40</sup> or a rarefied region at the buffer end<sup>20</sup>). The number of particles at the buffer  $N_B$  is controlled by a relaxation algorithm of the form  $\Delta N_B = (\Delta t / \tau_r) (\langle N_B \rangle - N_B)$ . Thus, the average number particles within  $B$  relaxes toward a certain imposed value  $\langle N_B \rangle$  over a typical relaxation time of  $\tau_r \sim O(100)$  MD time steps. The imposed average is set to  $\langle N_B \rangle = \alpha N_C$ , where  $\alpha$  is a constant (within the range  $0.5 < \alpha < 0.8$ ) and  $N_C$  is the number of particles according to the local density at overlapping CFD cell  $C$ . Particles crossing the buffer end are removed and, when required (i.e., if  $\Delta N_B > 0$ ), particles are inserted near the buffer end using the USHER algorithm.<sup>21</sup>

To conclude this section, it is important to note that the external momentum flux is imposed onto the extended particle system (MD+ $B$ ). As a consequence, in absence of external forces, the momentum of the extended system MD+CFD+ $B$  is conserved, but the momentum of the real sys-

tem (MD+CFD) is not. The size of fluctuations of the system's total momentum (MD+CFD) is, however, bounded by the finite size of  $B$ . In fact, for typical buffer sizes the error in momentum conservation is negligible. This fact was shown in Ref. 19 using water as working fluid and a buffer width of several molecules' diameter. More comments on the effect of buffer size are deferred to Sec. VI B.

## V. THE COMBINED TRIPLE-SCALE SCHEME

The idea underlying the combination of the AdResS and the HybridMD is to gradually increase the number of DOFs describing the system, as one approaches an atomistically described region of interest where molecular processes and hydrodynamics are intertwined in some multiscale phenomena.

As shown in Fig. 3, the combined AdResS-HybridMD scheme might be envisaged as an "onion type" model. The resulting scheme retains all the atomistic detail within a small all-atom core (the ex layer) seamlessly connected, through the transition layer (hyb), with a coarser particle description (the cg layer), which keeps part of the molecular information (e.g., structure), and finally coupling the whole particle system with the surrounding flow at larger scales, solved via continuum fluid dynamics (the CFD layer).

The purpose of any multiscale method is to reduce the computational cost involved in solving large systems where different phenomena are intertwined at different length scales. A way to estimate the reduction in computational cost that this combined model brings forth is given by the volume density of the number of DOFs. Consider a molecular fluid composed by molecules of mass  $m=Mm_0$  (in this work  $M=4$ ). The DOF density at the ex region is then  $3M\rho_m$ , it decreases by a factor  $M$  at the cg domain, and becomes  $(3+1)\rho_m/\langle N_c \rangle$  at the CFD domain. Here  $\langle N_c \rangle = \rho_m V_c$  is the mean number of molecules within one control cell of volume  $V_c$  and  $(3+1)$  corresponds to the cell momentum (vector) and its mass density. In hybrid simulations of molecular liquids, the cell volume  $V_c$  is set accordingly to the molecules' size, so that one typically gets  $\langle N_c \rangle \sim O(100)$ . Thus for the same volume, the solution of the CFD domain is  $O(100)$  faster than the particle (cg) domain. In passing from the cg to the ex model, the reduction in DOFs of course depends on the molecular liquid considered. Indeed, the efficiency of the present method increases with increasing molecular mass of the fluid, i.e., the speed-up ranges from a factor 10 for liquid water<sup>26</sup> to  $10^4$  for polycarbonate.<sup>1</sup>

### A. The buffer

As previously mentioned, the buffer region, which is an extension of the particle's system, is not a part of the system MD+CFD (in particular, in Fig. 3, cell Nos. 5 and 11 belong to the CFD domain). However, the buffer is a key component of the HybridMD scheme as it acts as a mass reservoir and it is also used to impose external forces into the MD region. The domain decomposition of the combined AdResS and HybridMD scheme can be designed in several ways depending on how the buffer is filled up. In this work the buffer is uniquely filled with cg particles. However, in principle, one

can also choose to enlarge the buffer, allowing part of the ex core and both the hyb and cg layers to be included within  $B$ . This second choice for the buffer decomposition shall be explored in subsequent works. The combined setup used in this work is illustrated in Fig. 3. The buffer is part of the cg layer, while the MD region contains the rest of the cg layer, the transition layer hyb and the ex (all-atom) core.

One of the objectives of the combined AdResS-HybridMD model is to facilitate the simulation of open systems formed by relatively large molecules. As explained in Ref. 20 particle insertions are done at the buffer domain. In order to avoid particle overlapping or sudden increase of the system's energy upon each molecule insertion, one needs an insertion procedure. To that end, Delgado-Buscalioni and Coveney developed an efficient algorithm, called USHER,<sup>21</sup> initially designed for spherical soft particles (e.g., Lennard-Jones), and latter generalized to water.<sup>22</sup> By adapting the AdResS model into the HybridMD setup, the buffer can be made of soft coarse-grained particles, which are quite easily inserted by the USHER algorithm overcoming characteristic problems, when applying it to explicit molecules directly. For instance, in the dense tetrahedral fluid, the USHER required only about five trials per inserted cg molecule, meaning that the CPU cost of particle insertion is negligible. In this way, the multiscale method can be applied to larger molecules.

Finally, the external force is imposed onto the buffer particles according to the spatial distribution  $g(x)$ ; i.e., the external force to the buffer particle  $i$  is  $\mathbf{f}_i^{\text{ext}} = g(x_i)\mathbf{F}^{\text{ext}}/\sum_{i \in BG}(x_i)$ , where  $x$  is the coordinate normal to the hybrid interface. In this work we have used a constant distribution  $g(x_i)=1$ . More elaborate choices for  $g(x)$  enable one to obtain a flat density profile across the whole buffer (see Ref. 40). The problem of the density profile shape in open fluid systems is well studied and it is possible to adapt the function  $g(x)$  to the requirements of the hybrid model used. The choice  $g(x)=1$  is perfectly suited for the purposes of this work (shear flow solved via a flux-exchange scheme).

### B. Transport properties: Matching viscosities

In order to connect the fluid model mixture shown at the top part of Fig. 3, with an external continuum description of the fluid, we need to ensure that the coarse-grained models (cg and hyb) have the same transport properties as the explicit model (ex), at least for those transport coefficients relevant to the sort of flow considered. For instance, to consistently impose into the all-atom core the shear stress resulting from a certain shear flow, one requires to match the viscosities of the cg and hyb models to that of the all-atom fluid, i.e.,  $\eta_{\text{cg}} = \eta_{\text{ex}}$  and  $\eta_{\text{hyb}} = \eta_{\text{ex}}$ .

However, as explained in Sec. III, the cg and hyb models were initially designed to fit the pressure and molecular structure (radial distribution) of the explicit fluid model at a certain density and temperature. As expected, due to softer effective interaction potentials, the coarse-grained fluid has a smaller viscosity than the explicit molecular fluid (cg molecules hence move faster). One thus therefore requires a way to increase  $\eta_{\text{cg}}$  without modifying either the pressure-density

relation or the temperature. This problem was solved using the Galilean invariant local “transverse dissipative particle dynamics” (TDPD) thermostat,<sup>32</sup> which enables us to increase the viscosity of the fluid by allowing a noncentral component of the DPD thermostating force appearing at each binary collision. This transversal component mimics the shear of those DOFs that were integrated out in the coarse-graining procedure. Due to orthogonality the TDPD thermostat, which preserves the hydrodynamics, can be used in a combination with the standard DPD thermostat.<sup>31</sup> This enables us to adjust at the same time two friction constants  $\zeta^{\parallel}$  and  $\zeta^{\perp}$  for the standard DPD and TDPD thermostats, respectively.<sup>32</sup>

As explained in Ref. 20 the HybridMD algorithm can be used as a rheometer. We used this method to calibrate the transversal friction coefficient  $\zeta^{\perp}$  so as to fit the viscosity of the explicit model. As an example, for the tetrahedral fluid at temperature  $T=1.0k_B/\epsilon$  and pressure  $p=2.0\epsilon/\sigma^3$  (the equilibrium molecular density is  $\rho_m=0.175\sigma^{-3}$ ), one gets  $\eta_{\text{ex}}=1.30m_0/(\tau\sigma)$ . Using a TDPD thermostat with  $\zeta^{\perp}=0.037m_0/\tau$ , in shear flow simulations of the cg fluid we obtained a similar viscosity. The viscosity does virtually not depend on  $\zeta^{\parallel}$ , which was set to  $\zeta^{\parallel}=0.05m_0/\tau$ . Interestingly the variation of viscosity with  $\zeta^{\perp}$  is linear (see Ref. 32). This fact is quite useful for the calibration of  $\zeta^{\perp}$  but, more importantly it permits to match the viscosity of the hyb model by doing a simple linear transformation of  $\zeta^{\perp}$  over the hyb layer (e.g., in the denser tetrahedral case, from  $\zeta^{\perp}=0.037m_0/\tau$  at the cg-hyb interface to  $\zeta^{\perp}=0$  at the hyb-ex one). A similar procedure was also applied in Ref. 41 to match the diffusion constants across the system using a position dependent Langevin thermostat, which, however, does not conserve hydrodynamics.

**Diffusion constants:** We also measured the diffusion constant of the cg fluid model and compared it with the ex model. In liquids the state dependence of the diffusion constant should follow that of the viscosity

$$D = \frac{k_B T}{c \pi \eta}, \quad (7)$$

where  $c$  is the coefficient of proportionality.<sup>42,43</sup> According to Eq. (7), in an ideal situation where  $c_{\text{ex}}=c_{\text{cg}}$ , the diffusion constants and viscosity could be matched simultaneously with a specific choice of  $\zeta^{\perp}$ . However, in practice this is not granted and fitting the viscosity of the cg molecules to the ex value, will not necessarily fit the mass diffusion values. For the dense tetrahedral case we obtained  $D_{\text{ex}}=0.054\sigma^2/\tau$  while (using  $\zeta^{\perp}=0$ )  $D_{\text{cg}}\approx 0.085\sigma^2/\tau$ . Using  $\zeta^{\perp}=0.037m_0/\tau$  (which matches  $\eta_{\text{cg}}=\eta_{\text{ex}}$ ), one gets  $D_{\text{cg}}=0.066\sigma^2/\tau$ , which is still about 20% larger. One needs to further increase the transversal friction to  $\zeta^{\perp}=0.101m_0/\tau$  to get  $D_{\text{cg}}=D_{\text{ex}}$ .

## VI. RESULTS

### A. Equilibrium

The hybrid explicit/coarse-grained fluid models were designed to keep consistency in the pressure-density equation of state.<sup>23,24</sup> On the other hand, the open boundary conditions used by the HybridMD method (see Ref. 15) have been

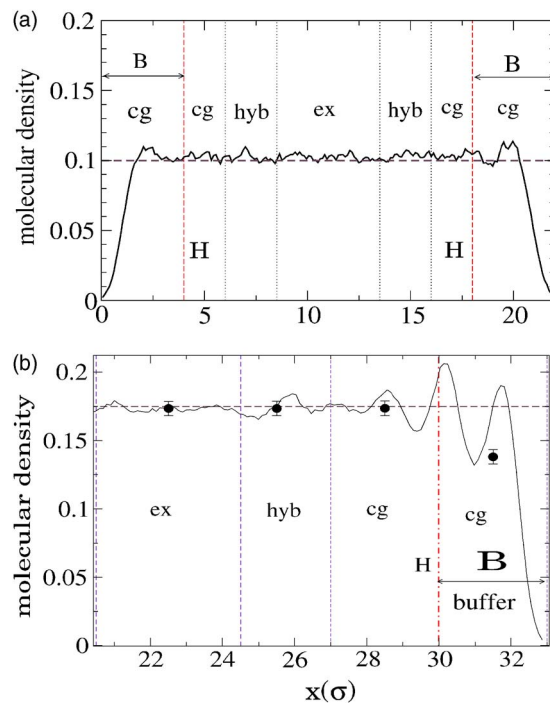


FIG. 4. (Color online) Molecular density profiles obtained from simulations of tetrahedral liquid at temperature  $T=1\epsilon/k_B$  and pressures (a)  $p=0.4\epsilon/\sigma^3$  and (b)  $2.0\epsilon/\sigma^3$ , corresponding to equilibrium molecular densities (shown in dashed lines) of  $\rho_m=0.1\sigma^{-3}$  and  $\rho_m=0.175\sigma^{-3}$ , respectively. The hybrid interfaces  $H$  (vertical dot-dashed line), buffer domains  $B$  and the subdomains of each fluid model (ex, hyb, and cg) are also indicated. The domain decomposition in (b) corresponds to that of Fig. 3 and circles correspond to the mean density at each control cell.

shown to reproduce the grand-canonical ensemble. This means that the combined AdResS-HybridMD model is already designed to keep consistency in the pressure-density relation. This fact is illustrated in Fig. 4, where the equilibrium density profiles in a hybrid simulation of tetrahedral fluid at temperature  $T=1\epsilon/k_B$  and two different pressures,  $p=0.4$  and  $2.0\epsilon/\sigma^3$  are shown. The mean densities at the molecular domain perfectly agree with the expected thermodynamic value (dashed lines in Fig. 4). In equilibrium, the mean values of the pressure, measured at each control cell of the molecular domain perfectly coincide with the external pressure imposed at the buffer. The oscillations in the density profile near and within the buffer domain observed in Fig. 4(b) are due to the way we are distributing the external pressure to the buffer particles [ $g(x)=1$ ]. As stated earlier, whenever required, it is possible to adapt the spatial distribution of the external force  $g(x)$  so as to obtain a flat density profile around the hybrid interface.<sup>40</sup> On the other hand, a small bump is also observed in the density profile at the hyb layer of Fig. 4(b) (the denser tetrahedral fluid). As discussed in Refs. 23 and 24, this is due to the force interpolation function used in the AdResS scheme. These small density oscillations have no effect on the transversal velocity profile (see Fig. 6, below), although, if necessary, they can also be further reduced using either an improved single point or multiple point versions of the “interface pressure correction” as explained in Refs. 24 and 41 to eventually obtain a flat profile.

To demonstrate that the local structure of the liquid is correctly reproduced in the molecular region of the triple-

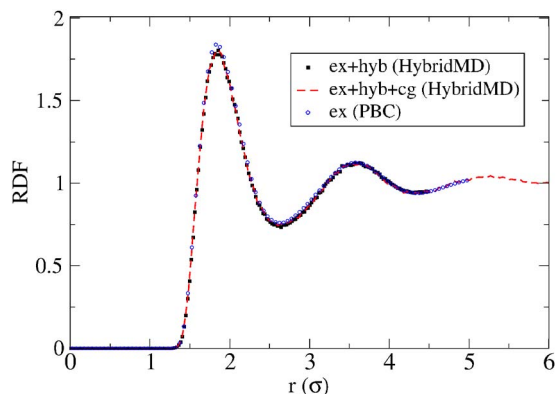


FIG. 5. (Color online)  $\text{RDF}_{\text{cm}}$ s of the liquid in the atomistic and transition domains (ex+hyb) and in the total molecular region (ex+hyb+cg) of the triple-scale model together with the reference  $\text{RDF}_{\text{cm}}$  of the all-atom system [ex(PBC)] from Ref. 24 at  $\rho=0.175/\sigma^3$ . All  $\text{RDF}_{\text{cm}}$ s match to the line thickness.

scale model we also show in Fig. 5 for the  $\rho_m=0.175/\sigma^3$  the center-of-mass radial distribution functions ( $\text{RDF}_{\text{cm}}$ s) of the molecules in the atomistic (ex) and transition (hyb) regimes and in the total molecular region of the triple-scale model together with the reference  $\text{RDF}_{\text{cm}}$  obtained from the all-atom simulation of the tetrahedral liquid.<sup>24</sup> All  $\text{RDF}_{\text{cm}}$ s match to the line-thickness indicating that the structure of the liquid in the molecular region is correct.

One of the most stringent tests for any model of open system is consistency with the thermodynamics of mass fluctuation. We calculated the standard deviation of the mass  $\sigma_N^2$  at the whole molecular system and at each control cell. In the thermodynamic limit one should get  $\sigma_N^2/V = \rho k_B T / c_T^2$ , where the isothermal sound velocity is  $c_T = (\partial P / \partial \rho)_T$  and  $V$  is the volume of the (sub)system considered. Intramolecular interactions across the interface of the volume induce deviations from the thermodynamic limit, which is recovered once the smallest length of the volume considered is made larger than at least three molecular diameters (for the tetrahedral model this is about  $6\sigma$ ). This was, in fact, shown in a previous work which considered an open HybridMD system of argon,<sup>20</sup> see also Ref. 44. In the low density tetrahedral fluid ( $\langle \rho_m \rangle = 0.1/\sigma^3, p = 0.4\epsilon/\sigma^3$ ), we get  $\sigma_N^2/V = 0.2m_0^2/\sigma^3$  for  $V = 15 \times 15 \times 5\sigma^3$ , while the thermodynamic limit is  $0.17m_0^2/\sigma^3$ . In the high density case ( $\langle \rho_m \rangle = 0.175/\sigma^3, p = 2.0\epsilon/\sigma^3$ ), larger deviations from the thermodynamic limit are due to increasing strength of interfacial intermolecular interactions:  $\sigma_N^2/V$  decreases from 0.27 to  $0.1m_0^2/\sigma^3$  as one increases the control volume from  $V = 15 \times 15 \times 3$  to  $V = 15 \times 15 \times 15\sigma^3$ , the thermodynamic limit being  $0.07m_0^2/\sigma^3$ . We also checked the continuity of mass fluctuation along the molecular domain, which is now composed by different fluid model layers (see Fig. 3). The standard deviation of density at different control cells are shown in Fig. 4 with error bars. They all coincide within the statistical accuracy. In the high density case using cells volume of  $V = 15 \times 15 \times 3\sigma^3$ , we get  $\sigma_N = 13.9m_0$ , in a cell containing ex fluid while  $\sigma_N = 14.5m_0$  in a cell containing cg fluid. Similar values are obtained in the hyb domains. This result indicates that the different fluid layers are in chemical equilibrium.

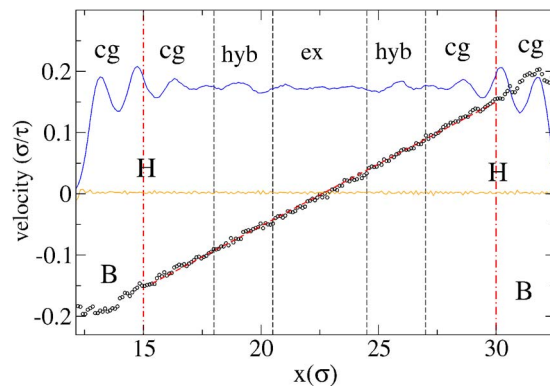


FIG. 6. (Color online) Velocity profile at the particle region of a hybrid simulation of a Couette flow of a tetrahedral fluid at pressure  $2.0\epsilon/\sigma^3$ . In the present setup the coarse-grained model (cg) and the hybrid fluid model (hyb) are placed inside the MD region, and their viscosities were tuned using the TDPD thermostat so as to match that of the explicit model (ex),  $\eta = 1.30m_0/(\tau\sigma)$ . The value of the DPD friction constants used for the cg and hyb fluids are  $\zeta^\perp = 0.037m_0/\tau$  and  $\zeta^\parallel = 0.05m_0/\tau$ , while at the ex model  $\zeta^\perp = 0.0$  and  $\zeta^\parallel = 0.05m_0/\tau$ . The dashed line corresponds to the expected linear velocity profile. The density (fluctuating around  $\rho_m = 0.175\sigma^{-3}$  in the molecular region) and the  $x$ -velocity (fluctuating around zero) profiles are also shown.

## B. Unsteady shear flow

In testing the hydrodynamic behavior of the AdResS-HybridMD model we first checked that the combined fluid model correctly transfers the transversal momentum across different model layers. To that end, we performed simulations of a simple Couette flow imposed in the  $y$  direction and analyzed the resulting steady velocity profile,  $\mathbf{v} = v_y(x)\mathbf{j}$ . Any significant difference in the fluid viscosity as one crosses from one model to another would induce a change in the slope of the velocity profile. The velocity profile of Fig. 6, obtained for the high density case shows, by contrast, a perfectly linear velocity profile with no slope change and in agreement with the expected Couette flow.

The second step was to test the response of the model to unsteady flow. We first considered the start-up of a Couette flow. Results of hybrid simulations using the high density tetrahedral fluid are shown in Fig. 7 and compared with the expected Navier–Stokes time-dependent solution. After more than about  $100\tau$  the system reaches the steady state; all the cells pertaining to the molecular domain (the system's setup corresponds to that of Fig. 3) closely follow the unsteady Navier–Stokes solution. We note that matching the viscosities of the different fluid models is a necessary but not sufficient condition to get the unsteady response right. A second issue, which needs to be considered, is any possible delay in the momentum transfer across  $H$ . Note that the external shear force, imposed at the buffer domain, corresponds to the local shear force at  $H$ . This momentum, however, takes a certain time to be diffused across  $B$  to reach the hybrid interface. This latency time is, to the first order, equal to  $\tau_B \sim l_B^2 \rho / \eta$ , where  $l_B$  is the width of the buffer in the normal direction to the  $H$  interface. Using  $l_B = 3\sigma$ , one gets  $\tau_B \sim 5\tau$ , which is quite a small time, in particular, it is 80 times smaller than the period of external forcing frequency ( $400\tau$ ). However,  $\tau_B$  increases quadratically with  $l_B$  so one needs to take into account any possible latency effect, especially if larger buffer

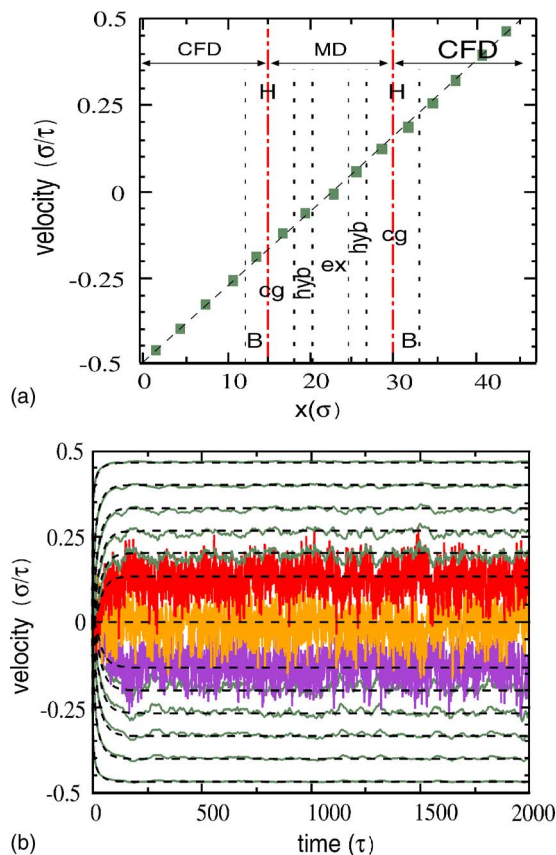


FIG. 7. (Color online) (a) Steady state velocity in a Couette flow of a tetrahedral fluid at pressure  $2.0\epsilon/\sigma^3$  and temperature  $T=1\epsilon/k_B$ . Filled circles correspond to the MD domain. (b) Start-up of the Couette flow showing the velocity at each control cell versus time; dashed lines corresponds to the deterministic Navier–Stokes solution. The setup corresponds to that of Fig. 3.

domains are need in simulations with larger molecules. In passing we note that this latency effect does not affect the final steady state (e.g., in a simple Couette flow).

We also performed simulations of oscillatory shear flow (the Stokes flow) arising as a consequence of the oscillatory motion of a wall along its plane direction. Figure 8 illustrates one example whereby a sinusoidal motion is imposed to one of the walls with a period of  $400\tau$ , while the other is kept at rest. Comparison with the full Navier–Stokes solution shows a quite good agreement and no trace of phase delay due to viscosity mismatches or by buffer size (here  $l_B=3\sigma$ ). In order to illustrate the latency effect induced by larger buffers, Fig. 9 shows a similar Stokes flow simulation, but now using a unique fluid throughout the particle system [a cg fluid with  $\langle\rho_m\rangle=0.175\sigma^{-3}$  and  $\eta=0.8m_0/(\tau\sigma)$ ] and a wider buffer  $l_B=5.5\sigma$ . In this case a small but appreciable phase delay is observed with respect to the full Navier–Stokes solution; as indicated in Fig. 9, the amount of time delay is of the same order as  $\tau_B\sim l_B^2\rho/\eta=25\tau$ .

## VII. CONCLUSIONS

We have presented a hybrid multiscale method, which combines a hybrid particle-continuum scheme<sup>19,20</sup> (HybridMD) with the particle-based hybrid atomistic-mesoscopic procedure (AdResS).<sup>23,24</sup> The resulting triple-

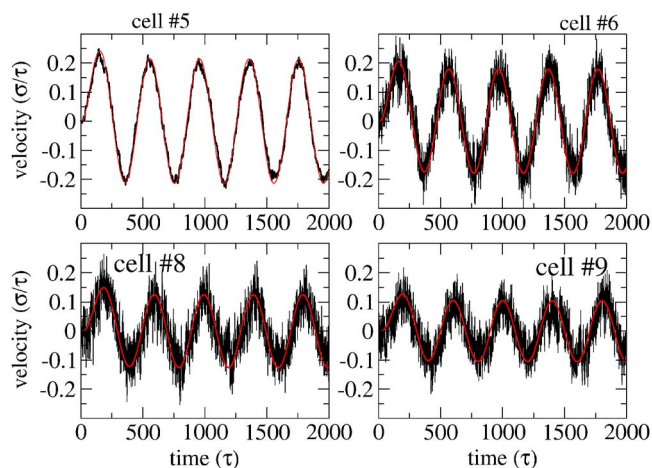


FIG. 8. (Color online) Velocity in the  $y$  direction at some selected cells (setup corresponds to that of Fig. 3) in a hybrid simulation of a Stokes flow: an oscillatory motion with a period of  $400\tau$  is imposed at the left wall while the right wall is kept at rest. Results from the nonfluctuating Navier–Stokes solution are also shown for comparison (solid lines).

scale model consists of a molecular particle-based micro-mesoscale region, which is divided into a central atomistic and a surrounding mesoscopic domain, and a macroscopic region described on the hydrodynamic continuum level. The combined scheme provides several important benefits. First, it greatly facilitates larger molecules insertion into an open molecular system, which is required by the HybridMD scheme. The combined scheme thus allows for simulations in the grand-canonical ensemble, using liquids composed by moderately large molecules. Second, it allows one to gradually increase the number of degrees of freedom as one focuses on a region of interest, described atomistically. In doing so, part of the molecular liquid description is kept in the coarse-grained level of detail, while only the mean flow is solved at the CFD layer. And finally, one of the problems

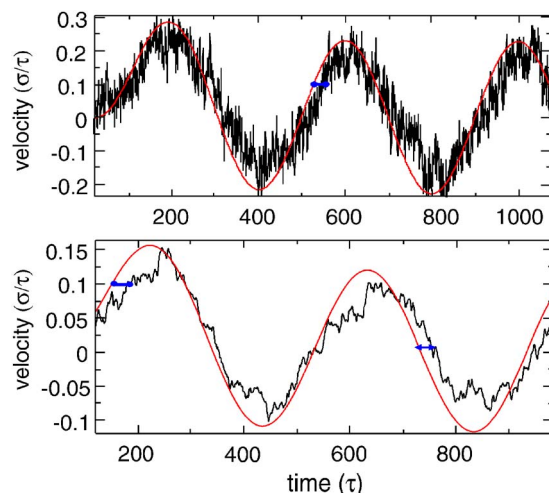


FIG. 9. (Color online) Velocity at the center molecular cell (top) and at one of the  $C$  cells (bottom) resulting from a Stokes flow simulation, with a period of  $400\tau$ . In this case a cg fluid model with  $\rho_m=0.175/\sigma^3$  and  $\eta=0.8m_0/(\tau\sigma)$  fills the whole particle system. The buffer size is  $l_B=5.6\sigma$ . Comparison with the full Navier–Stokes solution indicates a small phase delay of the hybrid solution. An estimate of the time delay  $\tau_B\sim l_B^2\rho/\eta$  is indicated with thick horizontal segments.

associated with the hybrid explicit/coarse-grained fluid model (AdResS) was the different viscosities of each fluid model. In this work we used the recently proposed TDPD (Ref. 32) to solve this problem. This allows to consistently couple the hydrodynamics of the whole (dual-scale) particle region with the continuum domain, using the HybridMD methodology.

In summary, the present methodology provides a new route for studying equilibrium and nonequilibrium processes in open molecular systems, involving liquids with relatively large molecules or even complex molecules in aqueous solutions.<sup>19,26</sup>

## ACKNOWLEDGMENTS

We thank Luigi Delle Site, Christoph Junghans, and Burkhard Dünweg for useful discussions. We also thank Anne Dejoan for valuable help in the hydrodynamics code. This work is supported in part by the Volkswagen foundation. R.D.-B. acknowledges additional funding from the Spanish government (MEC) Ramon y Cajal contract and Project No. FIS2007-65869-C03-01.

- <sup>1</sup>M. Praprotnik, L. Delle Site, and K. Kremer, *Annu. Rev. Phys. Chem.* **59**, 545 (2008).
- <sup>2</sup>H. Raffi-Tabar, L. Hua, and M. Cross, *J. Phys.: Condens. Matter* **10**, 2375 (1998).
- <sup>3</sup>J. Q. Broughton, F. F. Abraham, N. Bernstein, and E. Kaxiras, *Phys. Rev. B* **60**, 2391 (1999).
- <sup>4</sup>N. G. Hadjiconstantinou, *Phys. Rev. E* **59**, 2475 (1999).
- <sup>5</sup>J. A. Smirnova, L. V. Zhigilei, and B. J. Garrison, *Comput. Phys. Commun.* **118**, 11 (1999).
- <sup>6</sup>J. Rottler, S. Barsky, and M. O. Robbins, *Phys. Rev. Lett.* **89**, 148304 (2002).
- <sup>7</sup>G. Csanyi, T. Albaret, M. C. Payne, and A. DeVita, *Phys. Rev. Lett.* **93**, 175503 (2004).
- <sup>8</sup>A. Heyden, H. Lin, and D. G. Truhlar, *J. Phys. Chem. B* **111**, 2231 (2007).
- <sup>9</sup>S. T. O'Connell and P. A. Thompson, *Phys. Rev. E* **52**, R5792 (1995).
- <sup>10</sup>J. Li, D. Liao, and S. Yip, *Phys. Rev. E* **57**, 7259 (1998).
- <sup>11</sup>W. Cai, M. de Koning, V. V. Bulatov, and S. Yip, *Phys. Rev. Lett.* **85**, 3213 (2000).
- <sup>12</sup>E. G. Flekkoy, G. Wagner, and J. Feder, *Europhys. Lett.* **52**, 271 (2000).
- <sup>13</sup>P. Koumoutsakos, *Annu. Rev. Fluid Mech.* **37**, 457 (2005).
- <sup>14</sup>R. Delgado-Buscalioni, E. Flekkøy, and P. V. Coveney, *Europhys. Lett.* **69**, 959 (2005).
- <sup>15</sup>E. G. Flekkoy, R. Delgado-Buscalioni, and P. V. Coveney, *Phys. Rev. E* **72**, 026703 (2005).
- <sup>16</sup>X. Nie, M. O. Robbins, and S. Chen, *Phys. Rev. Lett.* **96**, 134501 (2006).

- <sup>17</sup>R. Delgado-Buscalioni and P. V. Coveney, *Physica A* **362**, 30 (2006).
- <sup>18</sup>A. Dupuis, E. M. Kotsalis, and P. Koumoutsakos, *Phys. Rev. E* **75**, 046704 (2007).
- <sup>19</sup>G. De Fabritiis, R. Delgado-Buscalioni, and P. Coveney, *Phys. Rev. Lett.* **97**, 134501 (2006).
- <sup>20</sup>R. Delgado-Buscalioni and G. De Fabritiis, *Phys. Rev. E* **76**, 036709 (2007).
- <sup>21</sup>R. Delgado-Buscalioni and P. V. Coveney, *J. Chem. Phys.* **119**, 978 (2003).
- <sup>22</sup>G. De Fabritiis, R. Delgado-Buscalioni, and P. V. Coveney, *J. Chem. Phys.* **121**, 12139 (2004).
- <sup>23</sup>M. Praprotnik, L. Delle Site, and K. Kremer, *J. Chem. Phys.* **123**, 224106 (2005).
- <sup>24</sup>M. Praprotnik, L. Delle Site, and K. Kremer, *Phys. Rev. E* **73**, 066701 (2006).
- <sup>25</sup>M. Praprotnik, L. Delle Site, and K. Kremer, *J. Chem. Phys.* **126**, 134902 (2007).
- <sup>26</sup>M. Praprotnik, S. Matysiak, L. Delle Site, K. Kremer, and C. Clementi, *J. Phys.: Condens. Matter* **19**, 292201 (2007).
- <sup>27</sup>C. F. Abrams, *J. Chem. Phys.* **123**, 234101 (2005).
- <sup>28</sup>D. Reith, M. Pütz, and F. Müller-Plathe, *J. Comput. Chem.* **24**, 1624 (2003).
- <sup>29</sup>M. Praprotnik, K. Kremer, and L. Delle Site, *Phys. Rev. E* **75**, 017701 (2007).
- <sup>30</sup>A hybrid molecule (hyb model) is composed of an all-atom molecule with an additional massless center-of-mass particle serving as an interaction site.
- <sup>31</sup>T. Soddemann, B. Dünweg, and K. Kremer, *Phys. Rev. E* **68**, 046702 (2003).
- <sup>32</sup>C. Junghans, M. Praprotnik, and K. Kremer, *Soft Matter* **4**, 156 (2008).
- <sup>33</sup>M. Praprotnik, K. Kremer, and L. Delle Site, *J. Phys. A: Math. Theor.* **40**, F281 (2007).
- <sup>34</sup>L. Delle Site, *Phys. Rev. E* **76**, 047701 (2007).
- <sup>35</sup>For the tetrahedral fluid we used  $\Delta t_c = 0.2\tau$ ,  $\delta t = 0.005\tau$ , and  $\Delta t = 0.1\tau$ , where  $\tau = (m\sigma^2/\epsilon)^{1/2}$  is the standard Lennard-Jones time unit for the monomer.
- <sup>36</sup>The traceless symmetric tensor is defined as  $A_{\alpha\beta}^S = (A_{\alpha\beta} + A_{\beta\alpha}) - (2/3)A_{\gamma\gamma}$ , where repeated index convention applies.
- <sup>37</sup>G. De Fabritiis, M. Serrano, R. Delgado-Buscalioni, and P. V. Coveney, *Phys. Rev. E* **75**, 026307 (2007).
- <sup>38</sup>Mass, momentum, and velocity at one MD cell,  $k$ , are  $M_k = \sum_{i \in V_k} m_i$ ,  $\mathbf{P}_k = \sum_{i \in V_k} m_i \mathbf{v}_i$ , and  $\mathbf{v}_k = \mathbf{P}_k / M_k$ , respectively.
- <sup>39</sup>In the present calculations continuity was enforced at the  $P$  cells, via the term  $(\langle \mathbf{v}_P^{\text{MD}} \rangle_{\Delta t_c} - \mathbf{v}_P^{\text{CFD}}) / \tau_r$ , with typically,  $\tau_r \cong O(\tau)$ . Here  $\langle \mathbf{v}_P^{\text{MD}} \rangle_{\Delta t_c}$  is the local mean particle velocity at  $P$ , time averaged over  $\Delta t_c$ , and  $\mathbf{v}_P^{\text{CFD}}$  is its corresponding CFD value, resulting from solving Eq. (6).
- <sup>40</sup>E. M. Kotsalis, J. H. Walther, and P. Koumoutsakos, *Phys. Rev. E* **76**, 016709 (2007).
- <sup>41</sup>S. Matysiak, C. Clementi, M. Praprotnik, K. Kremer, and L. Delle Site, *J. Chem. Phys.* **128**, 024503 (2008).
- <sup>42</sup>K. Kremer and G. S. Grest, *J. Chem. Phys.* **92**, 5057 (1990).
- <sup>43</sup>R. Brookes, A. Davies, G. Ketwaroo, and P. A. Madden, *J. Phys. Chem. B* **109**, 6485 (2005).
- <sup>44</sup>S. Torquato and F. H. Stillinger, *Phys. Rev. E* **68**, 041113 (2003).